Non-uniform strain measurement along a fiber Bragg grating using optical frequency domain reflectometry

Fangdong Zhu (朱方东)[1,2*], Dongsheng Zhang (张东生)[1,2], Peng Fan (樊 鹏)[2], Litong Li (李立彤)[2], and Yongxing Guo (郭永兴)[2]

[1]*Key Laboratory of Fiber Optic Sensing Technology and Information Processing, Wuhan University of Technology, Wuhan 430070, China*

[2]*National Engineering Laboratory for Fiber Optic Sensing Technology, Wuhan University of Technology, Wuhan 430070, China*

[*]*Corresponding author: zhufd_dream@163.com*

Received May 2, 2013; accepted August 2, 2013; posted online September 29, 2013

A novel method of measuring non-uniform strain along a fiber Bragg grating (FBG) using optical frequency domain reflectometry (OFDR) is proposed and experimentally demonstrated. This method can overcome the problems of traditional non-uniform strain measurement methods for FBGs, i.e., the likelihood of chirping and multiple peaking in the spectrum when FBG is subjected to inhomogeneous strain fields. Wavelength interrogation is realized by OFDR with a narrow-line-width tunable laser as the optical source. When non-uniform strain distributions along areas adjacent to structural damage are measured by this method, good agreement is obtained between measurements and theoretical simulation results.

OCIS codes: 060.2370, 060.2380, 070.2615.
doi: 10.3788/COL201311.100603.

Stress distributions along certain mechanical components can become extraordinarily complicated because of the sophisticated structures of modern mechanical equipment and the severe environments in which these components are used. Meanwhile, the structural characteristics and processing technologies of mechanical equipment are likely to generate stress concentrations and residual stresses, which result in complex non-uniform stress distributions along mechanical structures. Therefore, structural health monitoring of mechanical equipment must be shifted from uniform strain measurement to non-uniform strain measurement[1,2]. A fiber Bragg grating (FBG) is widely used in structural health monitoring because it is a highly rated new type of sensor with many advantages, including small size, light weight, immunity to electromagnetic interference, and capacity to form sensing networks using multiplexing technology[3−5]. When a FBG is subjected to homogeneous strain or temperature fields, the intensity response in the frequency domain exhibits a main peak at the Bragg wavelength. In this case, the sensing method is based on the tracking of the Bragg resonance peak shift[6,7]. However, the FBG itself occupies a certain length of 2–25 mm within which strain or temperature may not be homogeneously distributed. Moreover, the Bragg wavelength condition becomes a function of the position along the grating and causes chirp and multiple peaking on the FBG spectrum. Consequently, measurement errors occur because one FBG is mistakenly taken as several FBGs by tracking the Bragg wavelength. To avoid this problem, a novel method with extremely high spatial resolution is proposed and demonstrated in this letter for measuring non-uniform strain along a FBG using the optical frequency domain reflectometry (OFDR) technique[8−10].

The simplified model of the measurement system with a FBG using OFDR is shown in Fig. 1. In this setup, light from the tunable laser is split by a 3-dB coupler into two beams, which then reach the reflector and FBG. Reflected light from the reflector and FBG then interfere with each other at the 3-dB coupler, and the resulting interference signal is converted into an electrical signal by the photodetector.

We divide the grating with gauge length l into n uniform sections of length Δz, as shown in Fig. 1. Given that Δz is sufficiently small, we assume that strain distribution along each section of the FBG is uniform when subjected to external stress. Therefore, the interference between reflected lights of the entire FBG and reflector can be regarded as the interference superposition generated by n FBG sections interfering with the light beam reflected from the reflector.

According to the transfer matrix method based on coupled mode theory[11−13], light reflected from the entire FBG at a coupler can be expressed as

$$\begin{bmatrix} R_0 \\ S_0 \end{bmatrix} = \mathbf{T} \begin{bmatrix} R_n \\ S_n \end{bmatrix}; \quad \mathbf{T} = \mathbf{P}_G \cdot \mathbf{F}_1 \cdot \mathbf{F}_2 \cdots \mathbf{F}_i \cdots \mathbf{F}_n, \tag{1}$$

where R_0 and R_n are the amplitudes of the forward propagating mode at the detector side end and at the other end, respectively; S_0 and S_n are the amplitudes of the backward propagating mode at the detector side end and

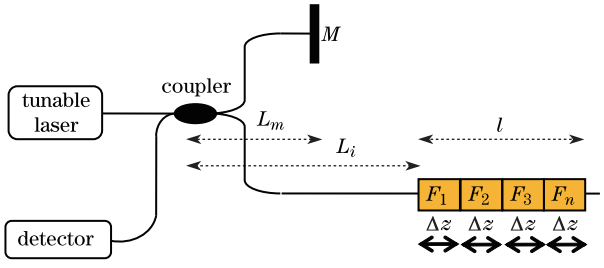

Fig. 1. Simplified model of measurement system using OFDR.

at the other end, respectively; $\mathbf{F}_i$ is the propagating matrix of FBG; $\mathbf{P}_G$ is the phase deviation matrix. $\mathbf{F}_i$ and $\mathbf{P}_G$ are given by

$$\mathbf{F}_i = \begin{bmatrix} \cosh(\gamma_{\mathrm{B}}\Delta z) - i\frac{\widehat{\sigma}}{\gamma_{\mathrm{B}}}\sinh(\gamma_{\mathrm{B}}\Delta z) & -i\frac{\kappa}{\gamma_{\mathrm{B}}}\sinh(\gamma_{\mathrm{B}}\Delta z) \\ i\frac{\kappa}{\gamma_{\mathrm{B}}}\sinh(\gamma_{\mathrm{B}}\Delta z) & \cosh(\gamma_{\mathrm{B}}\Delta z) + i\frac{\widehat{\sigma}}{\gamma_{\mathrm{B}}}\sinh(\gamma_{\mathrm{B}}\Delta z) \end{bmatrix}, \tag{2}$$

$$\mathbf{P}_G = \begin{bmatrix} \exp(-\mathrm{i}nkL_1) & 0 \\ 0 & \exp(\mathrm{i}nkL_1) \end{bmatrix}, \tag{3}$$

where n is the effective refractive index; $\widehat{\sigma}$ and κ are the direct current (DC) and alternating current self-coupling coefficients, respectively; $\gamma_{\mathrm{B}} = \sqrt{\kappa^2 - \widehat{\sigma}^2}$. When the boundary conditions of the coupled equation for FBG ($R_0 = 1$ and $S_n = 0$) are applied to Eq. (1), we obtain

$$RL_{\mathrm{FBG}} = S_0 = \frac{T_{21}}{T_{11}}. \tag{4}$$

Light reflected from the reflector at the coupler is given by

$$RL_m = \exp[\mathrm{i}(2nL_m k + \pi)], \tag{5}$$

where $k = 2\pi/\lambda$ is the light wavenumber, and L_m is the distance between the reflector and coupler.

The lights reflected from both FBG and reflector interfere with each other at the coupler, and the resultant interference signal is expressed as

$$RL_m + RL_{\mathrm{FBG}}. \tag{6}$$

Therefore, the interference signal intensity detected by the photodetector is given as

$$\begin{aligned} \mathrm{PD} &= (RL_m + RL_{\mathrm{FBG}})(RL_m + RL_{\mathrm{FBG}})^* \\ &= \{\exp[\mathrm{i}(2nL_m k + \pi)] + \sum_n R_i \exp(\mathrm{i}2nL_i k)\} \\ &\quad \{\exp[\mathrm{i}(2nL_m k + \pi)] + \sum_n R_i \exp(\mathrm{i}2nL_i k)\}* \\ &= (1 + \sum_n R_i^2) + 2\sum_n |R_i| \cos[2nk(L_i - L_m)] \\ &\quad + 2\sum_n^i \sum_n^j |R_i R_j| \cos[2nk(L_i - L_j)](i \neq j), \end{aligned} \tag{7}$$

where R_i is the reflective index of FBG section number i, and L_i is the distance between FBG section number i and the coupler. In Eq. (7), the first item of the polynomial is the DC signal, and the second is the superposition of the interference generated by light reflected from n sections of the FBG interfering with light from the reflector. In this case, we observe that the interference signal between each section of the FBG and the reflector is modulated by a specific frequency proportional to $L_i - L_m$. Therefore, the position of each section of the FBG can be determined from the frequency of the signal observed by the photodetector. The third item is the interference between sections of the FBG and is low-frequency interference. The application of a high-pass filter can eliminate the measurement errors generated by the first and third items. The light intensity signal can be converted into the position domain from the light wavenumber domain by applying a fast Fourier transform (FFT) expressed as

$$\begin{aligned} \mathrm{Fer}(l) &= \int_{k_1}^{k_2} (RL_m + RL_{\mathrm{FBG}})(RL_m + RL_{\mathrm{FBG}})^* \mathrm{e}^{-\mathrm{i}kl}\mathrm{d}k \\ &= \int_{k_1}^{k_2} (1 + \sum_n R_i^2)\mathrm{e}^{-\mathrm{i}kl}\mathrm{d}k + 2\pi \sum_n \{F_i[l - 2n(L_i - L_m)] \\ &\quad + F_i[l + 2n(L_i - L_m)]\} + 2\pi \sum_n^i \sum_n^j \{P_{ij}[l - 2n(L_i - L_j)] \\ &\quad + P_{ij}[l + 2n(L_i - L_j)]\}(i \neq j), \end{aligned} \tag{8}$$

where $F_i(l) = \int_{k_1}^{k_2} |R_i|\mathrm{e}^{-\mathrm{i}kl}\mathrm{d}k$ is the intensity of the reflected spectrum for FBG section number i by applying the FFT, and $P_{ij}(l) = \int_{k_1}^{k_2} |R_i R_j|\mathrm{e}^{-\mathrm{i}kl}\mathrm{d}k$ gives the interference intensity spectrum for FBG section number i and FBG section number j by applying the FFT; k_1 and k_2 are the initial and final light wavenumbers, respectively, as the laser scans[14].

The position domain information of FBG section number i is acquired using a narrow-band filter, rect (l), which has a band-pass area that includes only the position domain of FBG section number i, as

$$\begin{aligned} \mathrm{Fer}(l)\mathrm{rect}_i(l) = 2\pi\{&F_i[l - 2n(L_i - L_m)] \\ &+ F_i[l + 2n(L_i - L_m)]\}. \end{aligned} \tag{9}$$

Next, the wavenumber domain information of FBG section number i is exploited by applying an inverse FFT (IFFT) to position domain signal.

$$\begin{aligned} \mathrm{fer}_i &= \frac{1}{2\pi}\int_0^D \mathrm{Fer}(l)\mathrm{rect}_i(l)\mathrm{e}^{\mathrm{i}kl}\mathrm{d}l \\ &= 2|R_i(k)|\cos[2nk(L_i - L_m)], \end{aligned} \tag{10}$$

where D is the theoretical maximum distance that can be measured by this method.

Usually, an envelope curve of a narrow band signal is obtained by the Hilbert transform in digital signal processing. The Hilbert transform of a real function $s(t)$ is the convolution of $s(t)$ and $1/\pi t$, which is demonstrated as

$$\widehat{S}(t) = \mathrm{HT}[s(t)] = p(t) * s(t) = \frac{1}{\pi}\int_{-\infty}^{\infty} \frac{s(\tau)}{t - \tau}\mathrm{d}\tau. \tag{11}$$

As a phase delay $\pi/2$ is applied to the signal $\widehat{S}(t)$, an analytical function of $\widehat{S}(t)$ is expressed as

$$g(t) = s(t) + \mathrm{j}\widehat{S}(t). \tag{12}$$

In this case, the amplitude of $g(t)$ is the external contour line of $s(t)$ and given as

$$A(t) = \sqrt{s^2(t) + \widehat{S}^2(t)}. \tag{13}$$

Thus, the reflected spectrum intensity of FBG section number i is expressed as

$$A_i(k) = \sqrt{|2R_i(k)|^2\cos^2[2nk(L_i-L_m)]+|2R_i(k)|^2\sin^2[2nk(L_i-L_m)]} = 2\,|R_i(k)|\,. \quad (14)$$

According to the characteristics of Bragg grating, the wavelength corresponding to the maximum intensity on the reflected spectrum is the Bragg wavelength. When $k = k_0$, the maximum intensity of the reflected spectrum is obtained as

$$A_i(k)_{\max} = (2|R_i(k)|)|_{k=k_0}. \quad (15)$$

Consequently, the Bragg wavelength of FBG section number i is given by

$$\lambda_{\rm B} = \frac{2\pi}{k_0}. \quad (16)$$

Strain measurement along FBG section number i can be realized by tracking the Bragg wavelength shift. In this method, the entire FBG is divided into n sections, and the size of n is determined by the wavelength tuning range of laser. Therefore, strain measurement within a tiny area that cannot be realized by traditional demodulation method can be achieved by the proposed method.

An arrangement for measuring strain distribution along the FBG using OFDR is shown in Fig. 2. In this testing system, light from the laser is split into two beams by the 3-dB coupler C1. One beam is then sub-split into another two beams by coupler C3, the other reaches the FBG through the optical isolator (OIS) and coupler C4, and the light reflected by FBG interferes with the other beam at coupler C6. The interference signal is then converted into an electric signal by the photodetector (PD2), and then this electrical signal is acquired by the data acquisition card.

The other beam split by coupler C2 reaches the Mach–Zehnder interferometer composed of C2 and C5, as well as a fiber delay line (FD) for realizing nonlinear correction of the light frequency output from the laser[15]. We assume that the arm with the fiber delay line is L_{m1} long and referred to as the delay channel, whereas the other arm is L_{m2} long and referred to as the reference channel.

The optical signal within the delay channel is expressed as

$$RL_{m1} = \exp(\mathrm{i}2nL_{m1}k). \quad (17)$$

The optical signal within the reference channel is given as

$$RL_{m2} = \exp(\mathrm{i}2nL_{m2}k). \quad (18)$$

The resulting interference signal between the two channels detected by PD1 is given as

$$D = (RL_{m1} + RL_{m2})(RL_{m1} + RL_{m2})^*. \quad (19)$$

When Eqs. (17) and (18) are applied to Eq. (19), we obtain

$$\begin{aligned} D(k) &= \{\exp[\mathrm{i}(2nL_{m1}k)] + \exp[\mathrm{i}(2nL_{m2}k)]\} \\ &\quad \{\exp[\mathrm{i}(2nL_{m1}k)] + \exp[\mathrm{i}(2nL_{m2}k)]\}^* \\ &= 2[1+\cos(2nL_Mk)], \end{aligned} \quad (20)$$

where L_M is the path length difference between the two channels of interferometer and $L_M = L_{m1} - L_{m2}$. As the laser is tuned, Eq. (20) implies that the light intensity cyclically varies depending on the wavenumber change Δk given by

$$\Delta k = \frac{\pi}{nL_M}. \quad (21)$$

Equition (21) shows that Δk is a constant, which indicates that the interferometer linearly cycles as a function of wavenumber. The positive-approaching-zero crossing of the signal at PD1 is used to trigger the sampling of the signal at PD2. This phenomenon guarantees that the signal at PD2 is sampled at a constant wavenumber interval to realize nonlinear correction of light frequency output from the laser.

In this experiment, the wavelength tuning range of the laser is from 1 551.72 to 1 555.34 nm, the output power is 5 mW, the line width is 350 kHz, the wavelength stability is ±1 pm, and the data acquisition card uses NI-USB6251 with a maximum sampling rate of 1.25 M/s and 16-bit resolution.

The configuration of the aluminum tensile specimen used in this experiment is shown in Fig. 3. Fixed holes with a diameter of 11 mm exist on both ends of the test specimen, and a via hole with a diameter of 8 mm is designed on the tensile specimen, thereby generating a heterogeneous mechanical structure for the test specimen. Strain distribution along the areas adjacent to the hole becomes inhomogeneous when tension is applied to the test specimen. Force analysis of the specimen shown in Fig. 4 is implemented by finite element simulation using ANSYS. As a tension of 3 kN is applied to the free end of the test specimen while the other end of the test specimen is fixed, strain distribution along the test specimen is observed, as shown in Fig. 4. The color intensity, which indicates strain magnitude, shows that the strain distribution along the area adjacent to the via hole is inhomogeneous and that a relatively larger strain gradient occurs around the position where the via hole boundary is tangential to the loading direction.

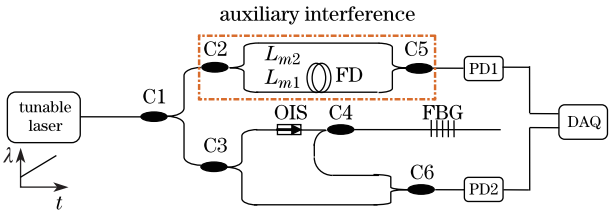

Fig. 2. Arrangement of measurement system along the FBG using OFDR.

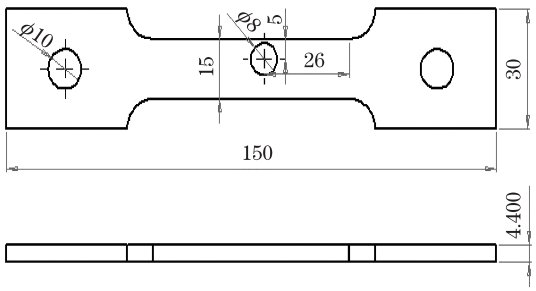

Fig. 3. Configuration of test specimen.

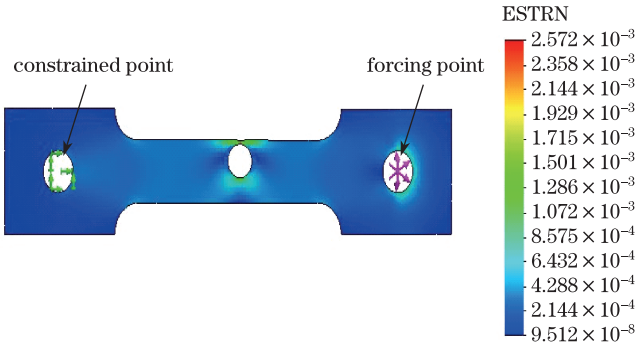

Fig. 4. Force analysis of test specimen.

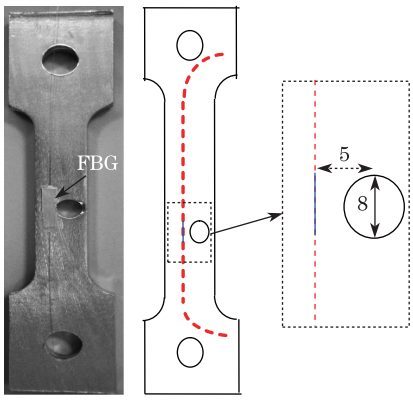

Fig. 5. Specimen with adhered FBG.

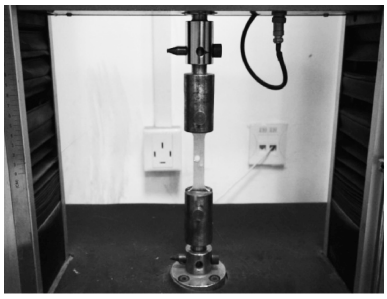

Fig. 6. Photograph of tensile experiment.

Figure 5 shows that a FBG with a length of 8 mm (Bragg wavelength of 1 553.47 nm) is stuck on the via hole boundary for 1 mm. Figure 6 shows that to eliminate any residual stress, prestretching of the test specimen is implemented. In other words, tensile loading is changed from 0 to 5 kN in steps of 1 kN, remaining at each step for at least 5 s, and then slowly decreasing to 0 kN. This process is repeated three times.

When prestretching is complete, non-uniform strain distribution along the hole boundary is measured with the FBG using OFDR. Based on this method, a tension of 3 kN is applied to one end of the test specimen with the other end of the test specimen fixed, and then the tunable laser starts to scan in the 1 551.72–1 555.34 nm range while the signal at PD1 is continuously acquired by the data acquisition card with a 400-kHz sampling rate. The positive-approaching-zero crossing of the signal at PD1 is determined by the LabView program and then used to trigger the sampling of the signal at PD2. The data acquisition process does not stop until the tunable laser finishes scanning.

Data processing is carried out to validate this method as follows. Firstly, a high-pass filtering process is applied to the data obtained at PD2 to eliminate the DC signal and low-frequency interference noise, and the resulting filtered signal is shown in Fig. 7. Secondly, the interference signal between the entire FBG and reflector is converted from the light wave domain to the position domain by applying the FFT to the filtered signal, as indicated in Fig. 8. Thirdly, as shown in Fig. 9, the domain position information of a certain section of the FBG is extracted from that of the entire FBG by applying a rectangular band-pass filter. Fourthly, the domain position information of a certain section of the FBG is converted to the light wave domain by applying IFFT, thereby obtaining the interference signal between this section of the FBG and the reflector, as shown in Fig. 10. Fifthly, the interference signal is processed by a Hilbert transform to obtain the envelope curve of the interference signal, which is the reflected spectrum of a certain section of

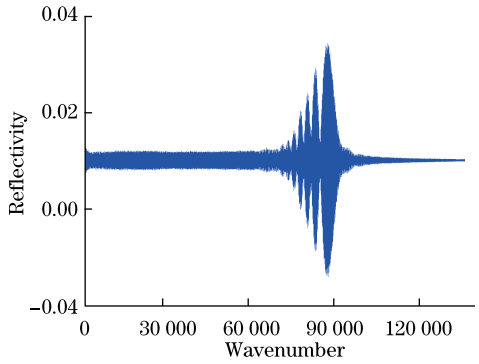

Fig. 7. Resulting filtered signal at PD2.

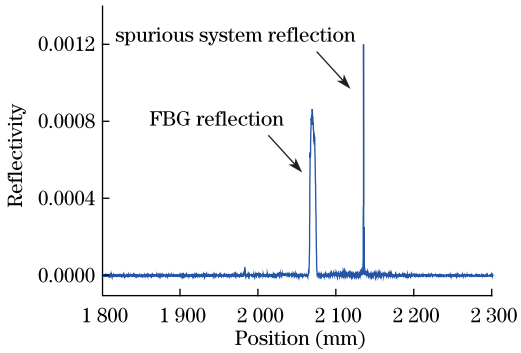

Fig. 8. Filtered signal applied by FFT.

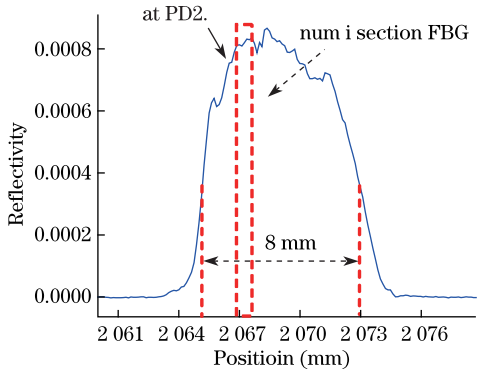

Fig. 9. Extracted domain position of FBG section i by narrow-band filtering.

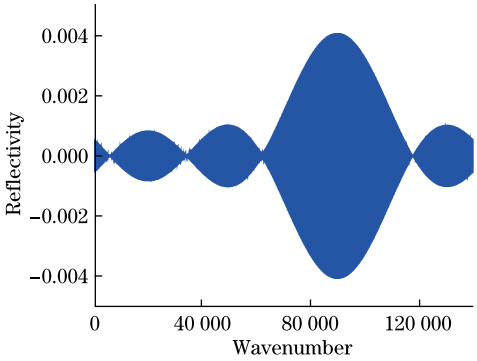

Fig. 10. Wavenumber domain of FBG section i by applying IFFT.

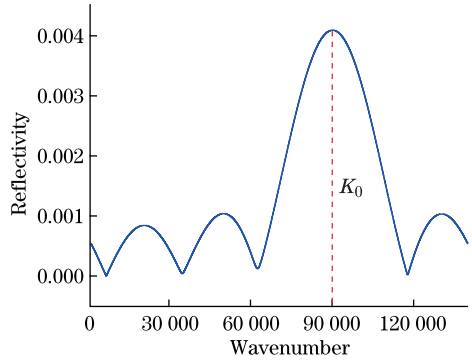

Fig. 11. Reflected spectrum of FBG section i.

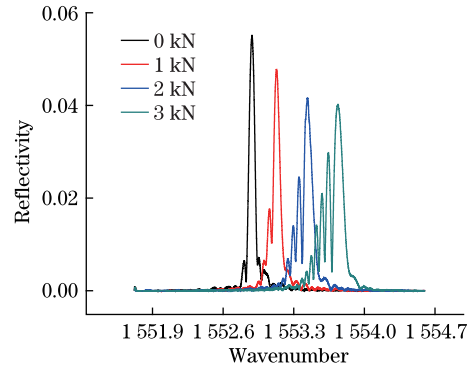

Fig. 12. Spectra of the FBG under different tensions.

the FBG, as indicated in Fig. 11. Sixthly and lastly, the Bragg wavelength is obtained from the light wavenumber corresponding to the maximum intensity of the reflected spectrum. Based on this processing method, the entire FBG can be divided into n FBG sections so that the spatial resolution is greatly improved.

Reflected spectra of FBG are exploited as tension 0, 1, 2, and 3 kN are applied, and the results are shown in Fig. 12. The horizontal axis indicates the wavelength and the vertical axis indicates the reflectivity. The FBG wavelength shifts in the long wavelength direction as the tension increases. When the tension is 0 kN, neither non-uniform strain along the FBG nor chirp or multiple peaks on the reflected spectrum are encountered, whereas more multiple peaks are encountered on the reflected spectrum as the tension increases. In particular, when a tension of 3 kN is applied, the reflected spectrum shape is broadened and splits into multiple peaks, which are mistakenly regarded as several gratings by the traditional measurement method, thereby causing the measurement errors.

Strain distributions along various positions of the FBG vary under different tensions, as shown in Fig. 13. The horizontal axis indicates the FBG position, and the vertical axis indicates the strain. The maximum strain is found at around the 4-mm point on the horizontal axis (the position where the FBG is tangential to the hole). Good agreement is observed between the actual measurement results and those of the finite element simulation.

Figure 14 compares the finite element simulation results with the strain distribution along the hole boundary measured by the FBG under a tension of 3 kN. The actual measurement results and the theoretical simulation results have the same strain distribution trend, whereas the theoretical simulation result is larger than the actual measurement result at the 4-mm point on the horizontal axis. One reason is that the grating is stuck onto the test specimen with adhesive, thus causing the strain transfer coefficient to be < 1. Another reason is that the positioning of the grating on the fiber cannot be accurately determined, thus making it impossible to stick the grating to the required position, and leading to measurement errors. Figure 14 shows that the position at which the Bragg grating is stuck offsets in the direction of one end of the test specimen by approximately 0.5 mm.

In conclusion, a novel method of measuring non-uniform strain along a FBG using OFDR is proposed. The overall feasibility of non-uniform strain measurement with this method is demonstrated for formula derivation and tension experiment. A non-uniform strain distribution along areas adjacent to structural damage is obtained, and good agreement with finite element

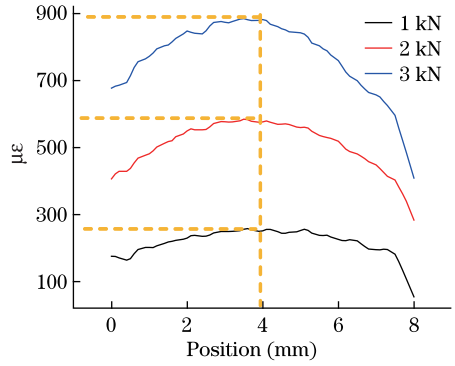

Fig. 13. Strain distribution along various FBG positions.

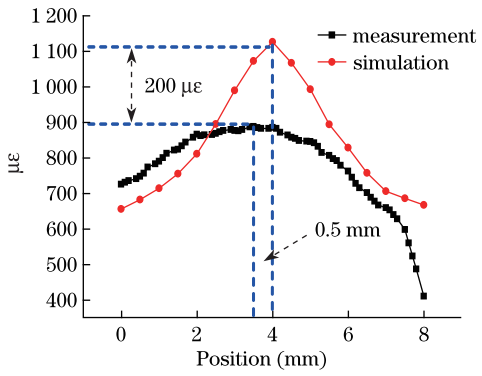

Fig. 14. Comparison between experiment and simulation results.

simulation is observed. This method can overcome the problems of traditional non-uniform strain measurement methods for FBGs, i.e., chirping and multiple peaking on the spectrum when the FBG is subjected to inhomogeneous strain fields. Therefore, this method clearly has great potential for future applications where local strain gradients can often arise.

This work was supported by the National High Technology Research and Development Program of China under Grant No. 2012AA041203.

References

1. P. Giaccari, G. R Dunkel, L. Humbert, J. Botsis, H. G Limberger, and R. P Salathe, Smart Mater. Struct. **14,** 127 (2005).
2. J. Zhang, Q. Sun, J. Wo, X. Li, and D. Liu, Chin. Opt. Lett. **11,** 020605 (2013).
3. H. Dong, J. Wu, and G. Zhang, Chin. Opt. Lett. **7,** 23 (2009).
4. Y. J. Rao, A. B. Lobo Ribeiro, D. A. Jackson, L. Zhang, and I. Bennion, Opt. Lett. **20,** 2149 (1995).
5. J. Liu, J. Zhang, X. Li, and Z. Zheng, Chin. J. Aeronautics (in Chinese) **24,** 607 (2011).
6. X. Zhang, Z. Meng, and Z. Hu, Chin. Opt. Lett. **9,** 110601 (2011).
7. Y. Zhan, S. Xue, and Q. Yang, Chin. Opt. Lett. **5,** 135 (2007).
8. B. Soller, D. Gifford, M. Wolfe, and M. Froggatt, Opt. Express **13,** 666 (2005).
9. M. Froggatt and J. Moore, App. Opt. **37,** 1741 (1998).
10. H. Igawa, K. Ohta, T. Kasai, I. Yamaguchi, H. Murayama, and K. Kageyama, J. Solid Mech. Mater. Eng. **2,** 1242 (2008).
11. T. Erdogan, J. Lightwave Technol. **15,** 1277 (1997).
12. M. Yamada and K. Sakuda, App. Opt. **26,** 3474 (1987).
13. G. Wang and Y. Wang, Chin. Opt. Lett. **9,** 090605 (2011).
14. M. A. Davis and A. D. Kersey, J. Lightwave Technol. **13,** 1289 (1995).
15. L. Lv, Y. Song, F. Zhu, and X. Zhang, Chin. Opt. Lett. **10,** 040604 (2012).